Estimation of fracture toughness of liver tissue: Experiments and validation

Can Gokgol, Cagatay Basdogan*, Demircan Canadinc

College of Engineering, Koc University, Istanbul 34450, Turkey

ARTICLE INFO

ABSTRACT

The mechanical interaction between the surgical tools and the target soft tissue is mainly dictated by the fracture toughness of the tissue in several medical procedures, such as catheter insertion, robotic-guided needle placement, suturing, cutting or tearing, and biopsy. Despite the numerous experimental works on the fracture toughness of hard biomaterials, such as bone and dentin, only a very limited number of studies have focused on soft tissues, where the results do not show any consistency mainly due to the negligence of the puncturing/cutting tool geometry. In order to address this issue, we performed needle insertion experiments on 3 bovine livers with 4 custom-made needles having different diameters. A unique value for fracture toughness ($J = 164 \pm 6\,\text{J/m}^2$) was obtained for the bovine liver by fitting a line to the toughness values estimated from the set of insertion experiments. In order to validate the experimental results, a finite element model of the bovine liver was developed and its hyper-viscoelastic material properties were estimated through an inverse solution based on static indentation and ramp-and-hold experiments. Then, needle insertion into the model was simulated utilizing an energy-based fracture mechanics approach. The insertion forces estimated from the FE simulations show an excellent agreement with those acquired from the physical experiments for all needle geometries.

© 2011 IPEM. Published by Elsevier Ltd. All rights reserved.

1. Introduction

The last two decades have witnessed significant advances in the fields of medical robotics, image-guided surgery, and computer-aided surgical planning and simulation. In all of these fields, accurate modeling of the interaction forces between surgical instruments and soft organ tissues has proven crucial for both the realistic simulation and the proper execution of the medical procedures. However, the precise estimation of these forces through a model requires the knowledge of material properties of the soft organ tissues targeted by the surgical instruments. While many of these properties have already been extensively examined, some are left unnoticed, such as fracture toughness, the resistance of a material to fracture. Only in a few exceptional studies, the emphasis was placed on estimating the fracture toughness of a soft biological material [1–6], investigating the geometrical effects of the instruments in tissue penetration through models based on fracture toughness [7], and measurement of the interaction forces via needle insertion experiments [8–10].

The fracture toughness of the soft tissue targeted by the surgical tools plays a critical role in medical procedures, such as catheter insertion, robotic-guided needle placement, suturing, cutting or tearing, and biopsy. Specifically, all these procedures involve tissue

damage to a certain extent, which should be kept to a minimum in order to avoid any medical complications [11–13]. Thus, the knowledge of fracture related material properties, especially the fracture toughness, is of utmost importance.

Despite the significant amount of work carried out to determine the fracture toughness of hard biomaterials, such as bone [14] and dentin [15], estimation of fracture toughness of the soft tissues has come under the focus of only a limited number of studies that mostly rely on a fracture mechanics approach based on energy balance [16,17]. For instance, Azar and Hayvard [1] inserted suture, syringe and biopsy needles with diameters ranging from 0.71 mm to 2.1 mm into porcine liver to calculate the crack size and the fracture toughness of the liver. In particular, two consecutive insertions were made into the same spot on the liver; the first one creating the crack and the second one being a free-pass. Then, the fracture toughness was calculated by taking the difference between the fracture and the viscoelastic works first, and then dividing the difference by the crack area. The calculated fracture toughness of the porcine liver varied between 75.8 and 185.6 J/m². Chanthasopeephan et al. [2], on the other hand, employed a scalpel as the cutting tool, and the fracture toughness of pig liver was estimated to vary between 186.98 and 224.83 J/m², with a standard deviation reaching to 142 J/m² in some experiments. Cutting with scissors was considered by Pereira et al. [3] to estimate the fracture toughness of the human skin, where samples were obtained from the hands of two cadavers. The fracture toughness of the dorsal skin was estimated as $1777 \pm 376\,\text{J/m}^2$ along the longitudinal

* Corresponding author. Tel.: +90 212 338 1721; fax: +90 212 338 1548.
  E-mail address: cbasdogan@ku.edu.tr (C. Basdogan).

direction and as $1719 \pm 674 \, \text{J/m}^2$ along the circumferential direction, while the palmar skin had an estimated fracture toughness of $2365 \pm 234 \, \text{J/m}^2$ along the skin creases and $2616 \pm 395 \, \text{J/m}^2$ across the skin creases. Comley and Fleck [4] estimated the toughness of porcine dermal and adipose skin tissue (soft connective tissue under the dermal layer) via a trouser tear test as $17{,}000 \, \text{J/m}^2$ and $4100 \, \text{J/m}^2$, respectively. Misra et al. [5] used an experimental set-up to robotically steer Nitinol needles having different diameters and bevel tips into 3 plastisol gels in different stiffnesses and a porcine gel. Using a single insertion, the rupture toughness of the plastisol gels, ordered in increasing stiffness, was estimated as 115.40, 218.19 and $221.04 \, \text{J/m}^2$. The rupture toughness of the porcine gel, on the other hand, was estimated as $82.28 \, \text{J/m}^2$. Utilizing a trouser tear test, Shergold [6] measured the fracture toughness of the silicone rubbers of grades Sil8800 and B452 as $3100 \, \text{J/m}^2$ and $3800 \, \text{J/m}^2$, respectively. In an attempt to corroborate their penetration models for sharp-tipped and flat-bottomed punches [18], Shergold and Fleck [7] carried out penetration experiments on skin and skin-like silicone rubber, where they investigated the effect of the punch-tip geometry on the mechanics of penetration based on the experimental data obtained in [6].

As reported in the literature review, the toughness values estimated in the earlier studies make up a wide range, partially due to the differences in the material properties of the subjects, and partially owing to the methods chosen for testing and evaluation. Although it is not uncommon for the material properties of samples extracted from different animals to show variation due to the individual differences, we hypothesize that part of the large variation in the estimated values is due to the neglected effect of the puncturing/cutting tool geometry on the measurements. In particular, we point out that, even though the energy method has been used to evaluate the fracture toughness of soft tissues in the earlier needle insertion studies, no attention has been paid to the role of needle geometry in these evaluations. To prove this hypothesis, needle insertion experiments were performed in the current study on 3 bovine livers with 4 custom-made needles having different diameters, and the relationship between the fracture toughness and the needle diameter was investigated in detail. In order to validate the experimental results, FE simulations of the needle insertion process were carried out in ANSYS. The good agreement between the computed and experimentally measured interaction forces indicated that the current approach could be successfully adopted in medical procedures that require precise control of tissue cutting forces.

2. Materials and methods

2.1. Theory

The insertion of a needle into a soft tissue can be investigated by dividing the process into multiple distinct phases [8,16,17,19,20]. The process starts with the deformation of the soft tissue under the force exerted by the needle (Fig. 1). Due to the viscoelastic nature of the soft tissue, this deformation continues until a certain threshold is reached in the relation between the viscoelastic work, W_v, and the fracture work, W_f. In particular, during the deformation phase, the value of W_v remains larger than the W_f. As the needle penetrates deeper into the soft tissue, the W_f starts to increase, and eventually becomes equal to the W_v. When the value of the W_f surpasses the value of the W_v, the needle punctures the tissue and rupture occurs. This marks a very brief change of state in the process of insertion; with the occurrence of rupture, the stage of pure deformation ends and a mixed stage of penetration and deformation starts (Fig. 1). At this stage, as the needle continues its movement through the soft tissue, the forces tend to increase until the needle comes to a
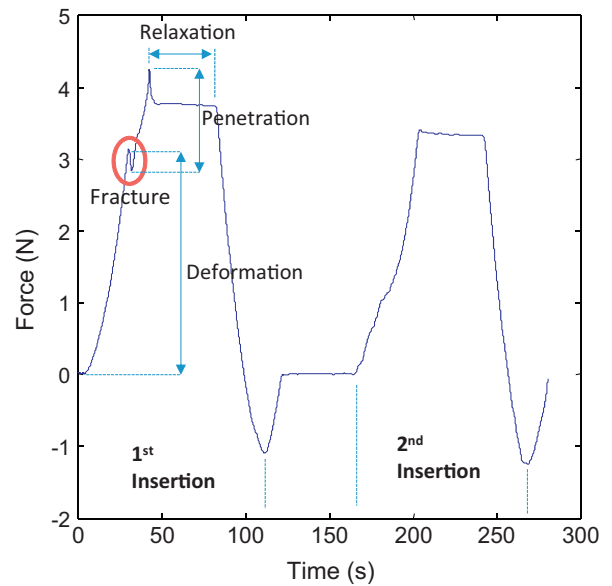

Fig. 1. The phases of needle insertion into soft tissue.

full stop. A phase of relaxation follows, as the motion of the needle comes to an end and the soft tissue remains in this phase until the needle is extracted from the tissue.

In order to determine the fracture toughness, J, via the energy balance equation, a method involving two subsequent insertions of a needle into the same spot was suggested in [8,17]. In the first insertion, all stages of insertion, namely deformation, rupture, and penetration, are present (Fig. 1). As a result, the energy balance equation for the first insertion is:

$$F_1 \, du = J \, d\Delta + d\Delta + P \, du \tag{1}$$

where F_1 is the force acting on the needle during the 1st insertion and du is the change in the needle displacement. Hence $F_1 \, du$ is the total work done by the needle during the first insertion, P is the friction force and $P \, du$ is the work done by friction. In Eq. (1), dA is the change in crack area (circumference of the needle times the incremental needle displacement, where the total crack area is the circumference times the current depth). Assuming that friction in the system is accounted for following the rupture, the sum of $J \, dA$ and the friction work becomes equal to the fracture work, W_f; whereas, $d\Delta$, the change in the strain energy, is equal to the viscoelastic work, W_v. As a result, the total work becomes equal to the sum of W_f and W_v.

During the second insertion to the same spot (Fig. 1), which is a free pass, only the penetration stage exists, such that the governing equation becomes:

$$F_2 \, du = d\Delta + P \, du \tag{2}$$

where F_2 is the force acting on the needle during the second insertion and has to be smaller than F_1. Since no rupture occurs during the second insertion, the value of fracture work is equal to zero. Since the change in strain energy, $d\Delta$, and the work done by friction, $P \, du$, are exactly the same for both insertions, the subtraction of Eq. (2) from Eq. (1) results in:

$$(F_1 - F_2) du = J \, dA \tag{3}$$

If the left and right hand sides of the above equation are integrated with respect to u, and the lower and upper limits of the integral are

Fig. 2. One of the 3 bovine livers used in the needle insertion experiments.

taken as the start and the end of the penetration stage, the fracture toughness can obtained from:

$$J = \frac{\int (F_1 - F_2) du}{\int dA} \qquad (4)$$

2.2. Experiments

The experiments were carried out on fresh bovine livers harvested from 3 different animals (Fig. 2). Rather than samples extracted from the livers; the livers were tested as a whole to minimize the blood loss and possible changes in the boundary conditions. Extra caution was paid to collect data from the same lobe of each liver and avoid muscle tissue during the insertion. All experimental data was collected within the first 2 h following harvesting.

An experimental set-up was established to characterize the hyper-viscoelastic material properties of the bovine livers via a cylindrical compression probe, followed by insertion experiments into the same livers with 4 separate needles each having different diameters to characterize their fracture toughness (Fig. 3). The major components of this custom-built set-up included a high-torque step motor moving the compression probe/insertion needle on a power screw, and a force sensor attached to its shaft [21].

In order to measure the strain-dependent hyperelastic and time-dependent viscoelastic responses, static indentation and ramp-and-hold experiments were performed on the livers, respectively, with the aid of a cylindrical probe having a round tip and a
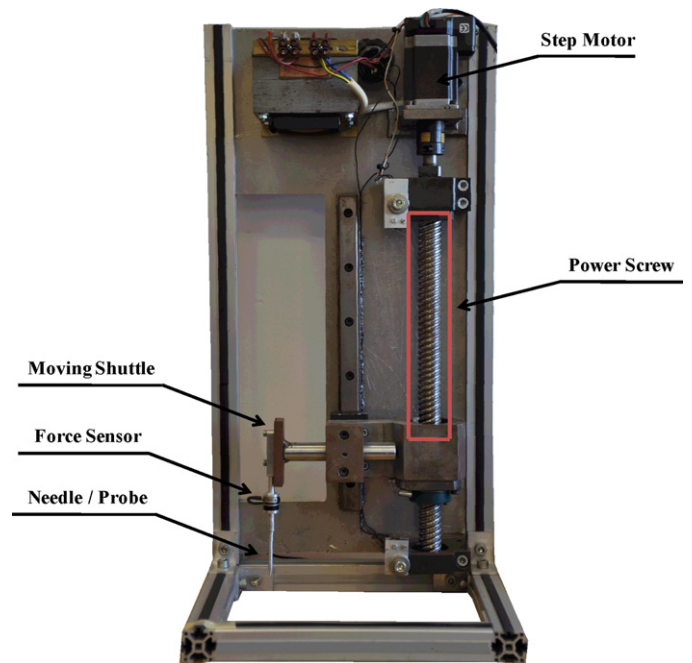

Fig. 3. The custom-built set-up for conducting characterization and fracture toughness experiments.

diameter of 6 mm (Fig. 4a). Then, to estimate the fracture toughness of the same livers, insertion experiments were performed using 4 different needles having sharp tips (Fig. 4a). The needle diameters were 2, 3, 4, and 5 mm, and the corresponding entry angles were 12°, 18°, 24° and 30°, respectively (as an example, the dimensions of the 2 mm needle are presented in Fig. 4b).

3. Results

In static indentation experiments performed with the cylindrical probe, the liver samples were compressed to a depth of 20 mm at a rate of 0.5 mm/s to eliminate the influence of viscoelastic and inertial effects, while the force response was measured by the force sensor (Fig. 5a). In ramp-and-hold experiments performed with the cylindrical probe, the livers were compressed to 20 mm within 1 s
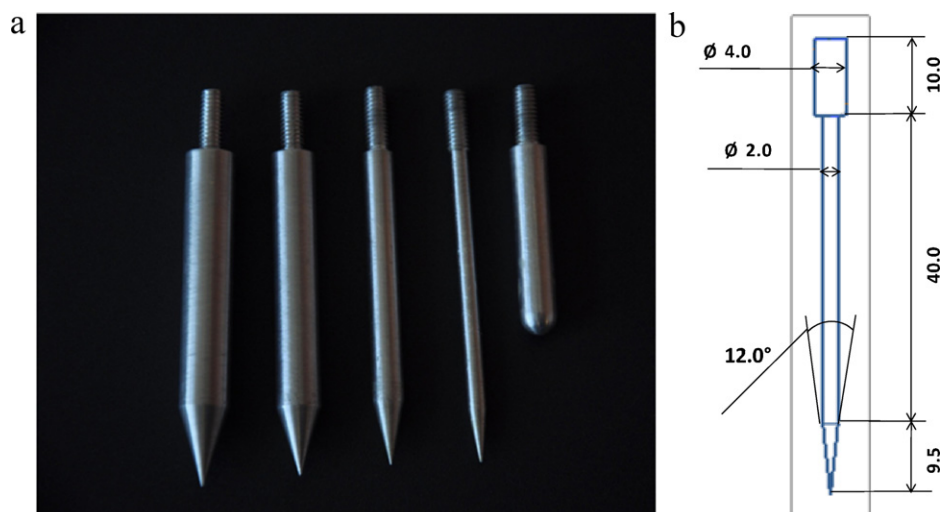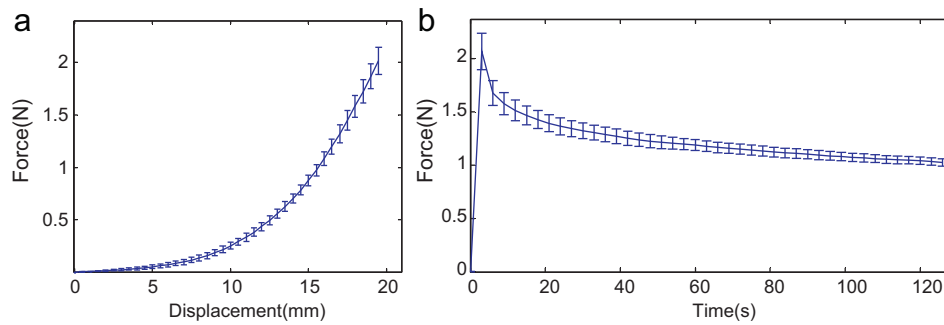

Fig. 4. (a) The four needles used in the fracture toughness experiments, and the cylindrical probe used in the characterization of hyper-viscoelastic material of bovine liver and (b) the technical drawing of the 2 mm needle.

Fig. 5. (a) The force response of bovine liver under static loading and (b) ramp and hold loading. The curves represent the averaged values obtained from 3 livers and the bars show the standard deviations.

and the probe was held in compressed position for 125 s to record the force relaxation response as a function of time (Fig. 5b).

In order to estimate the fracture toughness of the bovine livers, each needle was penetrated into a depth of 20 mm at a rate of 3 mm/s, and the force response was measured as shown in Fig. 6. Following a brief period of relaxation, the needle was retracted from the liver, only to be inserted once more into the same hole to measure the force response again. A total of 4 measurements were taken from the different sections of each liver, and the insertion experiment was repeated for 4 different needles. It should be noted that, even though the penetration depth was 20 mm in all measurements, the data was plotted up to the second rupture in Figs. 6a, b and d in order to emphasize the parallel nature of the curves following the initial rupture. Specifically, the force vs. displacement curve of the first insertion is parallel to that of the second one following the initial rupture. The fracture toughness was estimated by first integrating this difference over the needle displacement and then dividing it by the crack area (Fig. 7). The slope of each line in Fig. 7 provided the fracture toughness estimated for a particular

needle diameter. Accordingly, as the needle diameter increased, the fracture toughness decreased (Tables 1 and 2). This observation was also supported by the duration of the deformation stage in the force response curves shown in Fig. 6; as the needle diameter increases the duration of the deformation stage decreases, indicating that the liver exerted less resistance to larger needles.

The data presented in both Tables 1 and 2 suggested that the fracture toughness was a linear function of the needle diameter. An excellent agreement was obtained ($y = -29x + 164$, $R^2 = 0.981$) when the average values of the fracture toughness for 3 animals were plotted against the needle diameter (Fig. 8). Using the y-intercept of the fit line, the fracture toughness of bovine liver was estimated as $164 \pm 6\,\mathrm{J/m^2}$.

4. Validation

In order to validate the experimental results, a FE model of bovine liver was constructed in ANSYS and the insertion experiments were simulated for each liver to compare the force responses
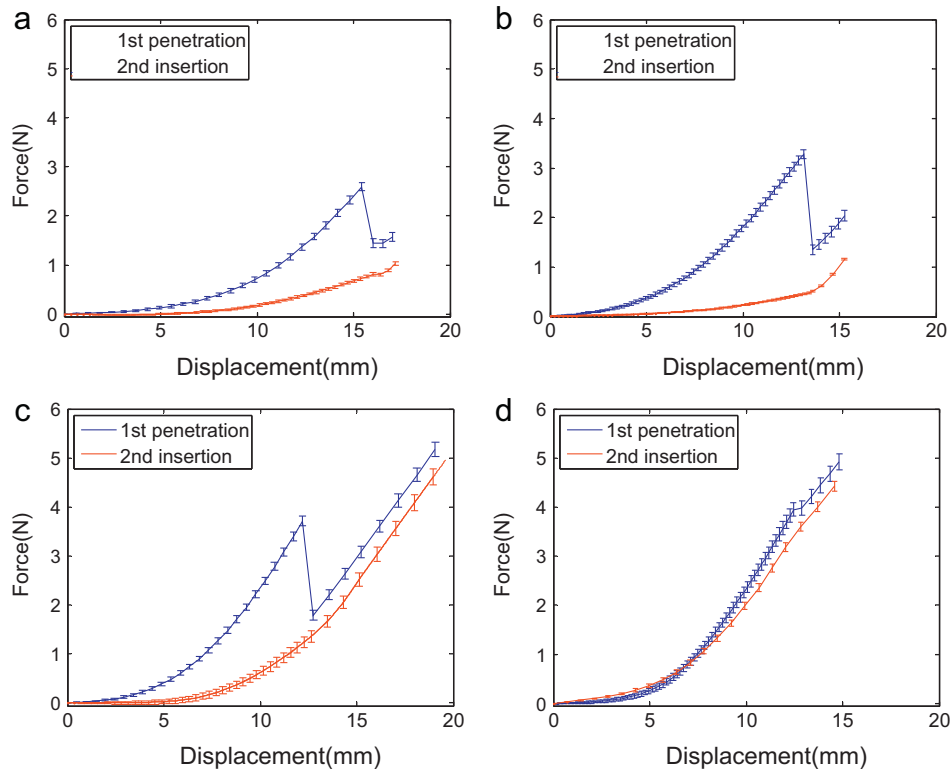

Fig. 6. The force–displacement responses of the bovine liver of Animal #1 for the needle diameters of 2 mm (a), 3 mm (b), 4 mm (c), and 5 mm (d). Each curve represents the average of 4 measurements performed on the liver and the bars show the corresponding standard deviations.

Table 1
The crack area (mm^2), the fracture toughness (J/m^2), and the fracture work (W_f) of the bovine livers for different needle diameters.

| Animal no.	Needle diameter (mm)	Parameters	Test no.			
			1	2	3	4
Animal #1	2	dA (mm^2)		8.07 ± 0.03		
		J (J/m^2)	120.3	107	113.5	116.55
		W_f (J)	970.82	863.49	915.95	940.56
	3	dA (mm^2)		24.88 ± 0.012		
		J (J/m^2)	73.85	69.32	65.62	70.85
		W_f (J)	1837.4	1724.7	1632.6	1762.7
	4	dA (mm^2)		78.74 ± 0.053		
		J (J/m^2)	46.94	41.98	43.92	45.21
		W_f (J)	3656.7	3352.0	3374.8	3638.6
	5	dA (mm^2)		36.35 ± 0.043		
		J (J/m^2)	24.79	21.49	22.23	22.89
		W_f (J)	901.11	781.16	808.06	832.05
Animal #2	2	dA (mm^2)		10.28 ± 0.23		
		J (J/m^2)	114.78	110.12	107.57	108.37
		W_f (J)	1179.9	1132.0	1105.8	1114.0
	3	dA (mm^2)		19.42 ± 0.14		
		J (J/m^2)	77.54	73.97	67.35	67.2
		W_f (J)	1505.8	1436.5	1307.9	1305.0
	4	dA (mm^2)		54.39 ± 0.041		
		J (J/m^2)	51.52	44.62	49.88	46.66
		W_f (J)	2802.2	2426.9	2713.0	2537.8
	5	dA (mm^2)		33.21 ± 0.039		
		J (J/m^2)	23.75	20.18	21.06	19.01
		W_f (J)	788.74	670.18	699.4	631.32
Animal #3	2	dA (mm^2)		11.42 ± 0.27		
		J (J/m^2)	112.42	103.77	105.23	110.43
		W_f (J)	1283.8	1185.1	1201.7	1261.1
	3	dA (mm^2)		25.94 ± 0.38		
		J (J/m^2)	71.94	68.1	65.89	75.99
		W_f (J)	1866.1	1767.6	1709.2	1971.2
	4	dA (mm^2)		57.37 ± 0.02		
		J (J/m^2)	50.21	45.27	41.44	42.94
		W_f (J)	2880.6	2597.1	2377.4	2463.5
	5	dA (mm^2)		38.94 ± 0.44		
		J (J/m^2)	22.85	16.25	19.82	21.72
		W_f (J)	889.78	632.78	771.79	845.78

Table 2
The average fracture toughness (J/m^2) of the bovine livers for different needle diameters.

| Needle diameter (mm)	Animal #1	Animal #2	Animal #3	Average
2	114.34 ± 5.62	110.21 ± 3.23	107.96 ± 4.12	110.83 ± 4.32
3	69.91 ± 3.42	71.52 ± 5.11	70.48 ± 4.44	70.63 ± 4.32
4	44.52 ± 2.09	48.17 ± 3.11	44.97 ± 3.32	45.88 ± 2.83
5	22.85 ± 1.41	21.00 ± 2.01	20.16 ± 2.89	22.33 ± 2.10
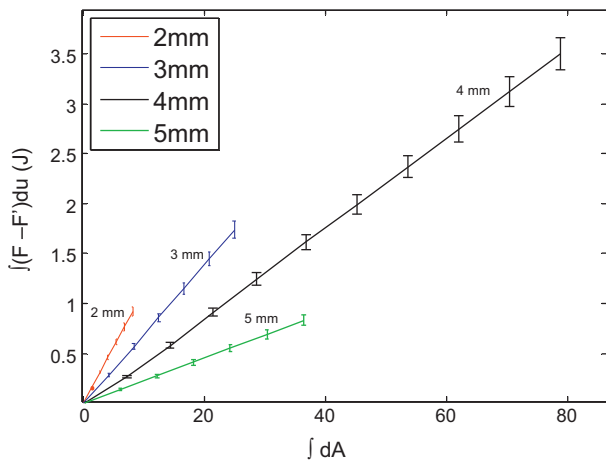
Fig. 7. The relationship between the fracture work and the crack area for different needle diameters. Each line is constructed based on the average of 4 measurements taken from the liver of Animal #1, and the bars show the standard deviations.
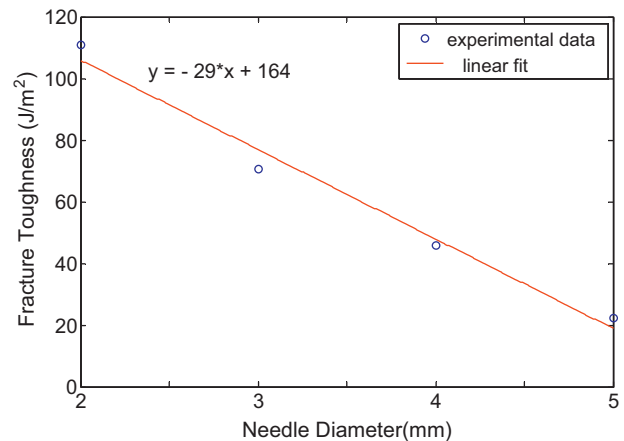
Fig. 8. The fracture toughness of bovine liver as a function of needle diameter. Each data point on the plot represents the average of the results obtained from 3 animals.
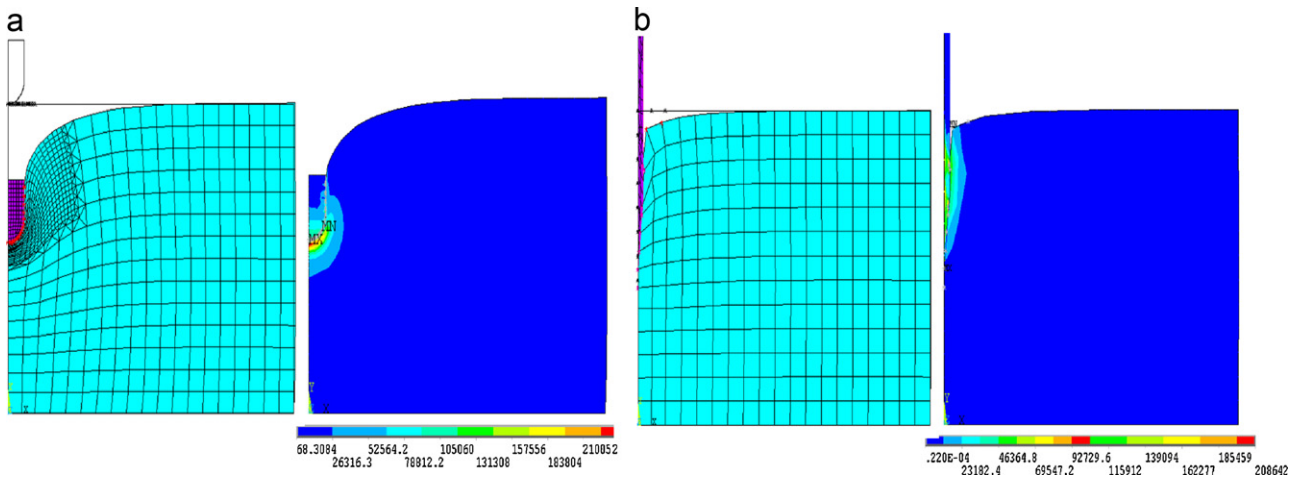
Fig. 9. The FE model of bovine liver deformed by the cylindrical probe having a round tip (a), and punctured by a needle having a sharp tip (b). The distribution of the von-Misses stress around the probe/needle forms intertwined circles.

estimated by the FE simulations with the experimentally measured ones. To reduce the computational load in FE simulations, a two-dimensional FE model was preferred over a three-dimensional one, and only the region around the contact was considered in the model, where the solution was assumed to be symmetric with respect to the axis of loading (Fig. 9). The base of the FE mesh was constrained to have zero displacement. The coefficient of friction between the contacting surfaces was set to 0.8, and the contact stiffness (FKN) and penetration tolerance (FTOLN) were set as 0.71 and 0.1, respectively. These parameters were determined by trial and error following the guidelines provided in ANSYS manual, such that the simulations could converge to a feasible solution and problems in contact profiling and distortion in the elements could be avoided.

Upon constructing the FE model, the hyper-viscoelastic material properties of each liver were determined by an inverse solution, such that the total error between the experimental force response and the simulated one was minimized through a set of optimization iterations as suggested in [22]. It should be noted that, since the experiments were performed with a cylindrical probe on a whole liver, it was not possible to obtain the material properties directly from the measurements. The Mooney–Rivlin strain energy function with 5 terms was employed to model the hyperelastic behavior of each liver:

$$W_{MRS} = C_{10}(I_1 - 3) + C_{01}(I_2 - 3) + C_{20}(I_1 - 3)^2 + C_{11}(I_1 - 3) + C_{02}(I_2 - 3)^2 \tag{5}$$

where $C_{10}, C_{01}, C_{20}, C_{11}$ and C_{02} are the hyperelastic material coefficients, and I_1 and I_2 stand for the principle invariants. For the sake of consistency with the experiments, the FE mesh was compressed to 20 mm by increments of 0.5 mm/step (Fig. 9a), and the hyperelastic material coefficients were optimized by the inverse solution, as tabulated in Table 3. The solution was iterated until the magnitude of the total error between the force response obtained from the physical experiments and the computed one was less than 0.05 N (Fig. 10a).

A Generalized Maxwell Solid (GMS) was used to model the viscoelastic behavior of the livers [21]. Then, the time-dependent relaxation moduli of the livers under ramp-and-hold strain input could be expressed analytically as:

$$E_R(t) = E_0 \left[1 - \sum_{j=1}^{N} \alpha_j\right] + E_0 \sum_{j=1}^{N} \alpha_j e^{-t/\tau_j} \tag{6}$$

where E_0 is the short-term elastic modulus, α_j represents the relative modulus, τ_j stands for the time constant, and N is the number of terms (i.e. Maxwell arms) used in the GMS model. For the sake of consistency with the experiments, an instantaneous displacement of 20 mm was applied to the FE mesh at the first time step of the simulations, and then the probe was held in position for the next 124 time steps (Fig. 9a) to estimate the optimum viscoelastic material coefficients through the inverse solution (Table 3). The inverse solution was iterated until the total error between the experimental relaxation force and the simulated one was less than 0.05 N (Fig. 10b). In our case, $N = 2$ returned satisfactory results (Table 3).

Following the estimation of the hyper-viscoelastic material properties of the livers, the insertion of the needles into the liver was simulated in ANSYS (Fig. 9b). In the FE model, besides the nodes at the base, the ones on the left boundary were also initially constrained to have zero displacement, but this constraint was released later on as the needle penetrated into the mesh. To be consistent with the experiments, each needle was inserted into a depth of 20 mm at a rate of 3 mm/step in the FE model. At each time step of the FE simulations, the total work done by the nodes at the contact interface was calculated using their displacement and the force acting on them. The fracture work, W_f, was calculated by multiplying the fracture toughness (Table 2) with the crack area, and the difference between the total work and the fracture work provided the viscoelastic work, W_v. When W_f exceeded W_v, the constraint on the node in contact with the needle was released, leading to the separation of that node from the boundary and further penetration of the needle into the mesh (Fig. 11). The simulated force response was recorded as a function of the penetration depth to compare it with the experimental data, as presented in Fig. 12.

5. Discussion

The results of the needle insertion experiments demonstrated that the fracture toughness was a linear function of needle diameter and a unique value could be estimated from the experimental data by curve fitting. Although the increase in force response as a function of needle diameter had been reported in [19] and different values of fracture toughness have been calculated for different needle diameters in [1], the relation between the needle diameter and fracture toughness had been overlooked in the literature so far. Furthermore, it is important to emphasize that the number of existing studies on fracture toughness of soft tissues is already very limited. Although the subjects and the methods chosen in some of the previous studies are different than that of our study, all the

Table 3
The hyper-viscoelastic material coefficients of the bovine livers estimated through the inverse FE solution.

Animal	C_{10}	C_{01}	C_{20}	C_{11}	C_{02}	α_1	α_2	τ_1	τ_2
#1	417.31	417.09	419.98	418.68	556.29	0.278	0.296	1.162	8.126
#2	456.40	416.24	417.82	418.24	716.83	0.351	0.278	0.978	10.573
#3	416.28	447.92	416.62	416.81	735.34	0.554	0.123	4.213	11.234
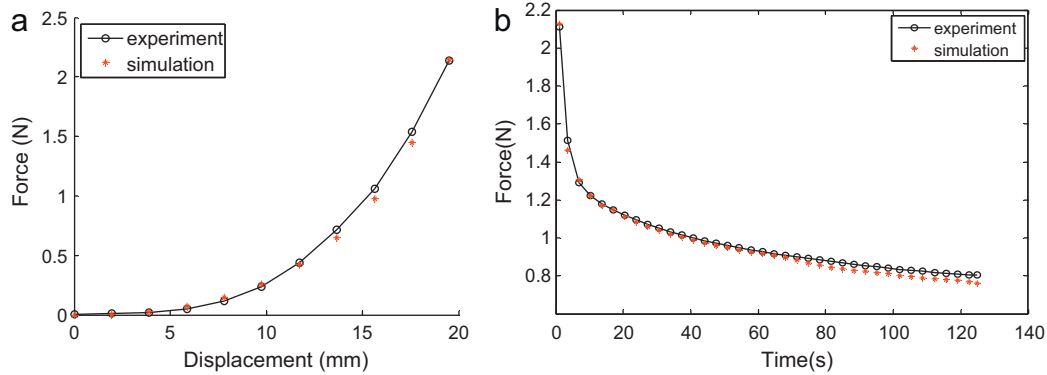
Fig. 10. The force–displacement (a) and force relaxation (b) responses of the bovine liver harvested from Animal #1 (solid circles), and the corresponding FE simulation results (red stars). (For interpretation of the references to color in this figure legend, the reader is referred to the web version of the article.)

previously reported fracture toughness values show large variations beyond the effect of material differences, suggesting that the influence of the cutting tool geometry on the fracture response has been neglected. In the current work, based on the experimental data collected from 3 animal livers, we estimated the fracture toughness of bovine liver as 164 J/m^2 with a standard deviation of 6 J/m^2. The mean value reported in this study for bovine liver is comparable to the ones reported for pig liver, yet the bounds of our toughness values are significantly tighter than the ones reported in earlier studies (varying between 75.8 and 185.6 J/m^2 in [1] and between 186.98
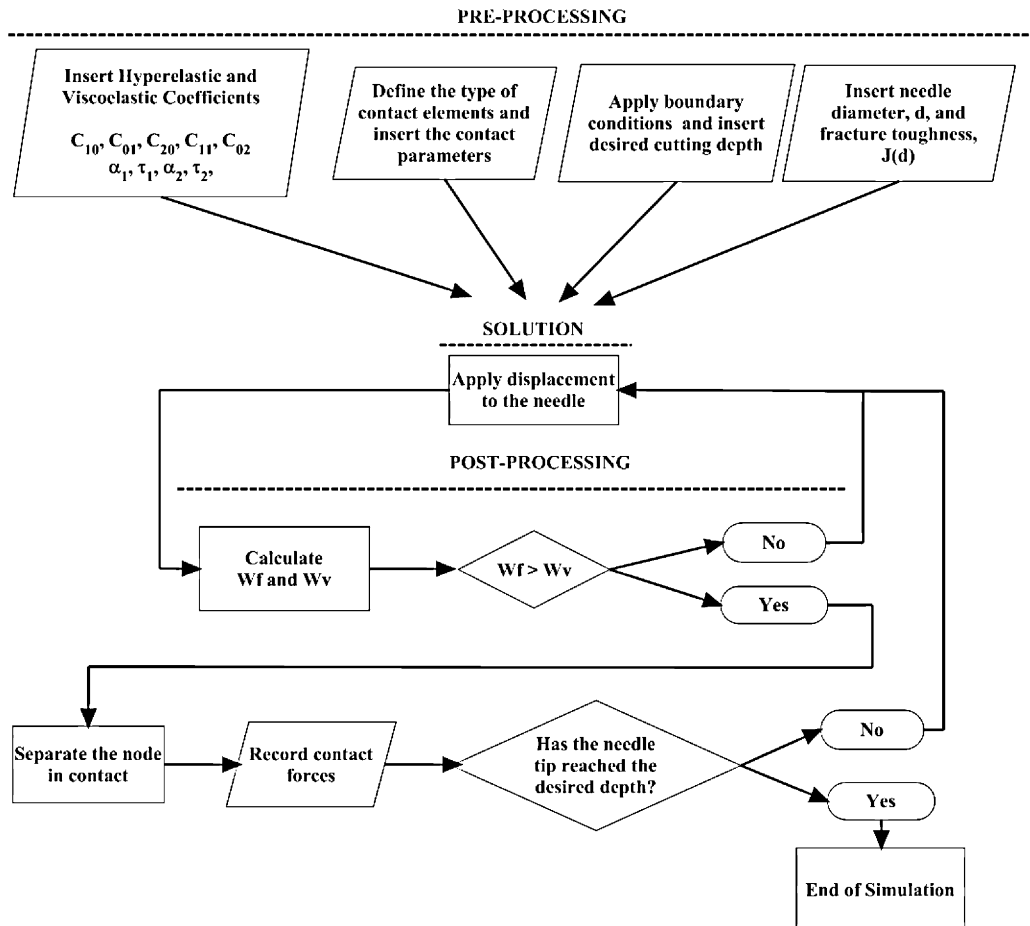
Fig. 11. The flowchart of needle insertion simulations in ANSYS.

Table 4
The fracture toughness (J/m^2) of the silicone sample for different needle diameters and insertion rates (note that each insertion experiment was repeated 4 times).
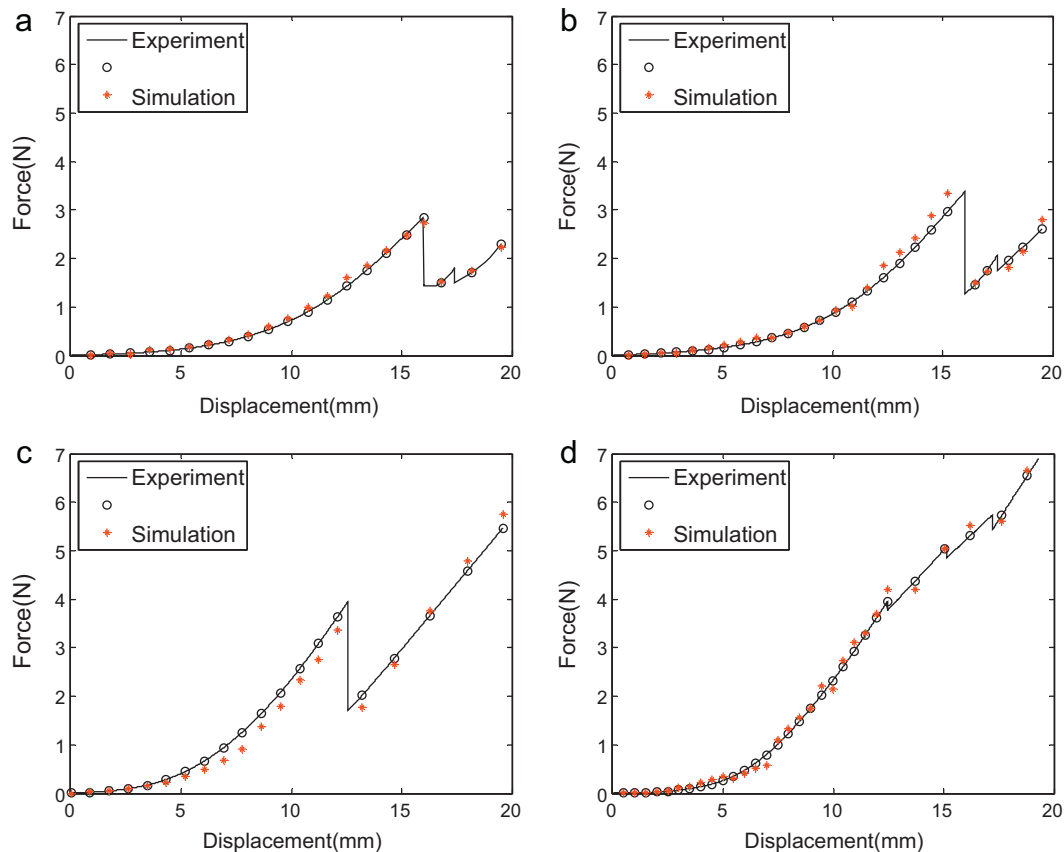
Insertion rate	Diameter			
	2 mm	3 mm	4 mm	5 mm
0.5 mm/s	146.18 ± 4.54	94.00 ± 2.73	59.00 ± 2.99	33.52 ± 0.44
3 mm/s	144.60 ± 3.25	87.10 ± 0.42	50.75 ± 0.21	26.05 ± 2.33
5 mm/s	140.80 ± 2.46	87.96 ± 2.89	48.88 ± 2.27	33.54 ± 0.96
Average	143.44 ± 4.06	90.00 ± 3.97	52.90 ± 5.35	32.16 ± 3.18

and 224.83 J/m^2 in [2]). The large variation reported in earlier studies could also be attributed to the differences in the measurement methods and devices. For example, in our preliminary experiments performed with thin syringe needles having diameters less than 2 mm, the recorded data was noisy due to the buckling of the needles and it was not possible to identify the distinct phases of the insertion in most of the trials. Thus, custom-made needles having diameters larger than a typical syringe needle were utilized in the current study to avoid noise and ensure more reliable data acquisition.

In order to validate the experiments on bovine liver and support the current hypothesis that the fracture toughness of a soft object depends on the needle diameter, we also conducted insertion experiments with a cylindrical silicone sample and investigated the effect of needle diameter on its fracture toughness (Fig. 13). The effect of insertion rate of the needle on the fracture toughness of the silicon sample was also investigated (Table 4). As in the case of bovine liver, there is a linear relation between the needle diameter and the fracture toughness of the silicon sample (Fig. 14). The y-intercept of the fitted line ($y = -37x + 210$, $R^2 = 0.962$) was used to estimate the fracture toughness of the silicone sample as

210 J/m^2. The results of this part of the study also suggested that the effect of insertion rate on the fracture toughness of the silicon sample was not significant, at least for the insertion rates used in the experiments (0.5 mm/s, 3 mm/s, and 5 mm/s).

A thorough set of FE simulations were performed in order to validate the experimental results on needle insertion. The force responses obtained from the FE simulations for different needle diameters showed an excellent agreement with the experimentally measured ones (Fig. 12). While the earlier studies also utilized FE techniques to simulate needle insertion into soft tissue [5,23–25], they mostly focused on modeling needle deformation rather than tissue deformation, and relied on linear FE models of soft tissue. Misra et al. [5] and Nienhuys and van der Stappen [23] developed hyperelastic FE models to simulate needle insertion into soft tissue, but the viscoelastic effects were neglected. Salcudean et al. [26] developed both linear and Neo-Hookean-based hyperelastic FE models of a deformable prostate and its surrounding tissue to simulate needle insertion during prostate brachytherapy, but again, viscoelastic effects were neglected. Only Mahvash and Dupont [27] utilized a linear Maxwell solid with $N = 1$ to investigate the viscoelastic response of soft tissue during needle

Fig. 12. The experimental and the computed force responses of the bovine liver harvested from Animal # 1 during the insertion of needles with diameters of (a) 2 mm, (b) 3 mm, (c) 4 mm, and (d) 5 mm.

Fig. 13. The cylindrical silicone sample tested in the validation experiments.

insertion. More importantly, most of the earlier studies did not integrate the material properties of a soft tissue measured experimentally into a FE model to validate the experimental data collected through the insertion experiments performed on the same tissue. Only Kobayashi et al. [28] developed non-linear and viscoelastic FE models of soft tissue in two dimensions to validate the results of their needle insertion experiments. In particular, different insertion depths and velocities were simulated to demonstrate that the simulation results agreed well with the experiments when both viscoelasticity and non-linearity were considered in the FE model.
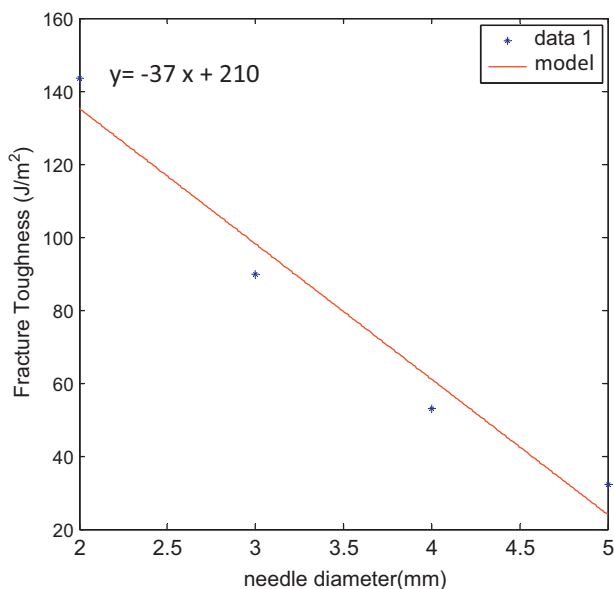

Fig. 14. The fracture toughness of the silicone sample as a function of needle diameter.

As for the fracture modeling techniques, Misra et al. [5] utilized a cohesive zone modeling approach while simulating the crack propagation within the tissue fracture zone. Specifically, the use of traction-separation laws to estimate the cohesive zone, and subsequently, the behavior of crack, suggest that the cohesive zone elements only represent cohesive forces, and thus, are placed between bulk elements. When these cohesive zone elements open, the crack propagation is simulated. As suggested by [29], fracture mechanics based modeling and cohesive zone modeling constitute the two most commonly utilized approaches for simulating crack propagation. The former adopts a mechanics point of view, which the authors have more experience with, and thus, was preferred in the current work. Thereby, the current study also provides an opportunity for comparing new results obtained from the fracture mechanics based modeling approach with those given by the cohesive zone modeling approach.

We have also made several modeling assumptions and simplifications to reduce the number of computations in our FE simulations. Even though the data was collected from whole livers in our experiments, only the immediate area around the tool contact was considered in the FE model. Furthermore, the FE model was constructed with two-dimensional axisymmetric elements to further reduce the number of computations. Moreover, during the FE simulations, we observed that it was not possible to achieve a perfect, non-penetrating contact in ANSYS. The penetration is controlled by two parameters in ANSYS; FKN, which defines the contact stiffness, and FTOLN, which is the penetration tolerance. In our simulations, FKN was the key parameter affecting the accuracy and the convergence of the solutions. Higher values of FKN reduced the penetration between the two surfaces, but caused convergence problems. On the other hand, lower values reduced the convergence problems by maximizing the penetration, but the results were unreliable due to the distorted elements in the mesh. Both parameters (FKN and FTOLN) were set by trial and error, such that there were no convergence and distortion problems.

Acknowledgement

Conflict of interest

The authors claim no conflict of interest.

References

[1] Azar T, Hayward T. Estimation of the fracture toughness of soft tissue from needle insertion. In: Proceedings of the 4th international symposium on biomedical simulations (ISBMS 2008). 2008. p. 166–75.
[2] Chanthasopeephan T, Desai JP, Lau ACW. Determining fracture characteristics in scalpel cutting of soft tissue. In: IEEE/RAS-EMBS conference on biomedical robotics and biomechatronics. 2006. p. 899–904.
[3] Pereira BP, Lucas PW, Teoh S-H. Ranking the fracture toughness of thin mammalian soft tissues using the scissors cutting test. J Biomech 1997;30:91–4.
[4] Comley K, Fleck NA. The toughness of adipose tissue: measurements and physical basis. J Biomech 2010;43:1823–6.
[5] Misra S, Reed KB, Douglas AS, Ramesh KT, Okamura AM. Needle–tissue interaction forces for bevel-tip steerable needles. In: Proc 2nd biennial IEEE/RAS-EMBS int conf biomed robot biomechatron. 2008. p. 224–31.
[6] Shergold OA. The mechanics of needle-free injection. Cambridge: Department of Mechanical Engineering, Cambridge University; 2004. p. 200.
[7] Shergold OA, Fleck NA. Experimental investigation into the deep penetration of soft solids by sharp and blunt punches, with application the piercing of skin. J Biomech Eng 2005;127(5):838–48.
[8] Heverly M, Dupont P. Trajectory optimization for dynamic needle insertion. In: Proceedings of IEEE international conference on robotics and automation (ICRA). 2005. p. 1658–63.
[9] Okamura AM, Simone C, O'Leary MD. Force modeling for needle insertion into soft tissue. IEEE Trans Biomed Eng 2004;51(10):1707–16.

[10] Frick TB, Marucci DD, Cartmill JA, Martin CJ, Walsh WR. Resistance forces acting on suture needles. J Biomech 2001;34:1335–40.

[11] Okazawa S, Ebrahimi R, Chuang J, Salcudean SE, Rohling R. Hand-held steerable needle device. IEEE/ASME Trans Mechatron 2005;10(3):285–96.

[12] DiMaio SP, Salcudean SE. Interactive simulation of needle insertion models. IEEE Trans Biomed Eng 2005;52(7):1167–79.

[13] Chong SY, Chong LA, Ariffin H. Accurate prediction of the needle depth required for successful lumbar puncture. Am J Emerg Med 2010;28:603–6.

[14] Wang X, Puram S. The toughness of cortical bone and its relationship with age. Ann Biomed Eng 2004;32(1):123–35.

[15] Yan J, Taskonak B, Platta JA, Mecholsky JJ. Evaluation of fracture toughness of human dentin using elastic–plastic fracture mechanics. J Biomech 2008;41:1253–9.

[16] Abolhassani N, Moallem M. Needle insertion into soft tissue: a survey. Med Eng Phys 2007;29(4):413–31.

[17] Atkins AG, Mai Y-W. Elastic and plastic fracture, metals, polymers, ceramics, composites, biological materials. Ellis Horwood Limited; 1985.

[18] Shergold OA, Fleck NA. Mechanisms of deep penetration of soft solids, with application to the injection and wounding of skin. Proc Roy Soc Lond A 2004;460:3037–58.

[19] Okamura AM, Simone C, O'Leary MD. Force modeling for needle insertion into soft tissue. IEEE Trans Biomed Eng 2004;51(10):1707–16.

[20] Maurin B, Barbé L, Bayle B, Zanne P, Gangloff J, de Mathelin M, et al. In vivo study of forces during needle insertions. In: Proceedings of the medical robotics, navigation and visualization scientific workshop (MRNV). 2004. p. 415–22.

[21] Ocal S, Ozcan MU, Basdogan I, Basdogan C. Effect of preservation period on the viscoelastic material properties of soft tissues with implications for liver transplantation. ASME J Biomech Eng 2010;132(10):101007, 7 pp.

[22] Samur E, Sedef M, Basdogan C, Avtan L, Duzgun O. A robotic indenter for minimally invasive measurement and characterization of soft tissue behavior. Med Image Anal 2007;11(4):361–73.

[23] Nienhuys H-W, van der Stappen FA. A computational technique for interactive needle insertions in 3d nonlinear material. In: Proceedings of IEEE international conference on robotics and automation (ICRA). 2004. p. 2061–7.

[24] Goksel O, Dehghan E, Salcudean SE. Modeling and simulation of flexible needles. Med Eng Phys 2009;31(9):1069–78.

[25] Hing JT, Brooks AD, Desai JP. Reality-based needle insertion simulation for haptic feedback in prostate brachytherapy. In: Proceedings of IEEE international conference on robotics and automation (ICRA). 2006. p. 619–24.

[26] Dehghan E, Salcudean SE. Needle insertion parameter optimization for brachytherapy. IEEE Trans Robot 2009;25(2):303–15.

[27] Mahvash M, Dupont PE. Mechanics of dynamic needle insertion into a biological material. IEEE Trans Biomed Eng 2010;57(4):934–43.

[28] Kobayashi Y, Onishi A, Watanabe H, Hoshi T, Kawamura K, Fujie MG. Experimental validation of viscoelastic and nonlinear model of liver for needle insertion simulation. In: Proceedings of IEEE international conference on biomedical robotics and biomechatronics. 2008. p. 469–76.

[29] ANSYS® Academic Research, Release 11.0, Help System, Structures with Material Non-Linearities, Cohesive Zone Material Models. ANSYS, Inc.